Dalton Transactions

ROYAL SOCIETY OF CHEMISTRY

COMMUNICATION

View Article Online
View Journal

Cite this: DOI: 10.1039/d5dt01320h

Received 5th June 2025,
Accepted 17th July 2025

DOI: 10.1039/d5dt01320h

rsc.li/dalton

Strong second-harmonic generation response in an organic–inorganic hybrid antimony bromide†

Xuemei Wen, Gangji Yi, Qinglan Zhong, Caihong Guo,* Hongmei Zeng, Guohong Zou and Zhien Lin *

A new organic–inorganic hybrid antimony bromide has been prepared using planar nicotinic acid as a structure-directing agent. The compound features a one-dimensional perovskite structure with a strong second-harmonic generation response (SHG) of 3.7 times that of KH_2PO_4. Theoretical calculations were performed to reveal the origin of its SHG response.

Second-harmonic generation (SHG) in metal halide perovskites is of current interest for its promising applications in laser technologies.[1] Most research has concentrated on the lead halide system, primarily because lead ions readily form octahedral coordination with halide ions.[2] Prominent examples in this field include [(*R*/*S*)-3-aminopiperidine]PbI_4, (*R*/*S*-2-MPD)PbX_3 (X = Cl, Br, I), and (L-ipp)(L-pro)PbI_3.[3] In contrast, the study of SHG-active antimony halide perovskites has been relatively limited. This may stem from the tendency of antimony halides to form centrosymmetric structures, as well as the difficulty of inducing the formation of SbX_6 octahedra rather than SbX_3 pyramids, SbX_4 disphenoids, and SbX_5 square pyramids.[4] Various synthetic parameters, including solvent type, organic structure-directing agents, pH, reaction duration, and temperature, have been investigated to manipulate the structures of antimony halides. For instance, centrosymmetric $(C_9H_{26}N_3)_2Sb_4Cl_{18}$ and noncentrosymmetric $(C_9H_{26}N_3)SbCl_6$ were obtained by studying the effect of different conformations of pentamethyldiethylenetriamine on antimony chlorides structures.[5] The noncentrosymmetric phase shows a moderate SHG intensity of 1.3 times that of KH_2PO_4 (1.3× KDP), which originates from the $SbCl_6$ octahedra.

An effective strategy to enhance the SHG responses of organic–inorganic hybrid solids is to exploit the synergistic effect of planar organic cations and various inorganic anions.[6] The rich chemistry of planar organic molecules offers many opportunities to design and synthesize new nonlinear optical (NLO) materials. In the early studies, the effect of guanidinium cation has been extensively studied to mimic the structural feature of the notable BO_3 unit.[7] Recently, π-conjugated pyridine derivatives (*e.g.*, 4-hydroxypyridine) have garnered significant attention due to their large hyperpolarizabilities and polarizability anisotropies.[8] For instance, Wang *et al.* reported the ultraviolet NLO crystal (3-AMP)$ZnBr_4$ by combining 3-(aminomethyl)pyridinium cations with tetrahedral $ZnBr_4^{2-}$ anions, achieving a strong SHG response of 4.36× KDP.[9] The integration of Me_3TPA (TPA = tri(pyridin-4-yl) amine) cations and trigonal planar AgX_3^{2-} anions has yielded the silver halides [Me_3TPA][AgX_3]X (X = Cl, Br, I) with remarkable SHG responses of 6.2–7.6× KDP.[10] Despite these advancements, the use of planar pyridinecarboxylic acids in the synthesis of SHG-active metal halide perovskites remains underexplored, even though these organic molecules can serve as linkers in constructing metal–organic frameworks with NLO properties.[11]

In this work, we investigate the structure-directing role of nicotinic acid as a representative of pyridinecarboxylic acids in the synthesis of organic–inorganic hybrid antimony bromides. Two new compounds, formulated as $(C_6H_6NO_2)_2Sb_2Br_8\cdot H_2O$ (**1**)‡ and $(C_6H_6NO_2)_2SbBr_5$ (**2**), were obtained in an effort to explore how the Sb/Br ratio influences crystal structures. Single crystal X-ray diffraction (XRD) analysis shows that compound **1** has a 0D tetrameric structure, while compound **2** features a zigzag 1D perovskite structure. Notably, compound **2** exhibits a strong SHG response of 3.7× KDP, which stands out among organic–inorganic hybrid antimony halide perovskites. First-principal calculations were performed to elucidate the origin of its SHG response.

Single crystals of compounds **1** and **2** were harvested by a solvent evaporation method (Fig. 1). For compound **1**, $SbCl_3$ (0.114 g, 0.5 mmol), nicotinic acid (0.062 g, 0.5 mmol), HBr (228 μL, 2 mmol), and methanol (1.5 mL) were mixed in a 10 mL glass beaker. After slow evaporation at 45 °C for two days, block crystals were obtained with a 45% yield based on

---

College of Chemistry, Sichuan University, Chengdu 610064, P. R. China.
E-mail: guocaihong@scu.edu.cn, zhienlin@scu.edu.cn

† Electronic supplementary information (ESI) available: Powder XRD patterns, TGA curves, IR spectra, UV-vis absorption spectra, birefringence measurements, DFT calculations, and additional figures. CCDC 2456325 and 2456326. For ESI and crystallographic data in CIF or other electronic format see DOI: **https://doi.org/10.1039/d5dt01320h**

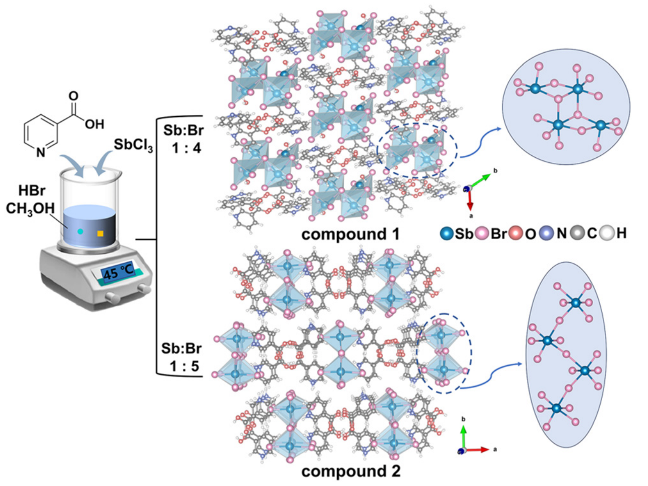

Fig. 1 Schematic diagram of the crystal growth conditions and structures of compounds **1** and **2**.

antimony. Similarly, when the amount of HBr was increased to 285 μL (2.5 mmol) while keeping other conditions the same, plate crystals of compound **2** were obtained with a 65% yield based on antimony. The experimental powder XRD patterns of compounds **1** and **2** are in good agreement with the calculated patterns simulated from the single-crystal XRD data analysis, verifying that the samples are phase pure (Fig. S1†). The thermogravimetric analysis (TGA) shows that the weight loss below 65 °C for compound **1** may be attributed to the departure of water molecules (Fig. S2†). The weight loss between 125 and 241 °C is attributed to the decomposition of the nicotinic acid molecules, the departure of HBr, and the sublimation of $SbBr_3$. For compound **2**, it remains thermally stable up to 120 °C. The weight loss between 120 and 252 °C is caused by the decomposition of the nicotinic acid molecules, the departure of HBr, and the sublimation of $SbBr_3$. IR spectra were collected to identify the functional groups existing in the structures of compounds **1** and **2** (Fig. S3†). The peaks at 3514 cm^{-1} should be attributed to the stretching vibrations of the O–H, verifying the presence of water molecules in compound **1**. The observed bands at 1632 cm^{-1} (for **1**) and 1590 cm^{-1} (for **2**) belong to the C=O stretching vibrations. The C–O stretching vibrations appear at 1296 cm^{-1} (for **1**) and 1280 cm^{-1} (for **2**). The UV-vis absorption spectra reveal that the optical bandgaps for compounds **1** and **2** are 2.87 eV and 2.80 eV, respectively (Fig. S4†). The difference in the band gap values may be due to their different structures and different Sb : Br ratios that they have. These values are comparable with those of organic–inorganic hybrid antimony bromines, such as $(TMA)_3Sb_2Br_9$ (2.95 eV), (2cepyH)$SbBr_4$ (2.82 eV), and $(TMP)_2(SbBr_5)(SbBr_3)$ (2.60 eV).[12] The birefringence of compounds **1** and **2** is measured using a Zeiss Axio A1 Scope polarizing microscope. The experimental values are determined to be 0.068@546 nm and 0.044@546 nm, respectively (Fig. S5†).

Compound **1** crystallizes in the centrosymmetric triclinic space group $P\bar{1}$ (no. 2). The asymmetric unit consists of two antimony atoms, eight bromine atoms, two protonated nicotinic acid molecules, and one water molecule. Of the two independent antimony atoms, Sb(1) atom is octahedrally coordinated by six bromine atoms, while Sb(2) atom is coordinated to five bromine atoms to form a square pyramidal geometry. Two $SbBr_6$ octahedra and two $SbBr_5$ square pyramids share common bromine atoms to give rise to a tetranuclear cluster. The Sb–Br bond distances are in the region of 2.5186(11)–3.2537(10) Å, which is consistent with other reports.[13] It is worth noting that mono-, di-, and tri-coordinated bromine atoms coexist in the tetrameric structure. The antimony bromide clusters interact with protonated nicotinic acid cations and water molecules through extensive N(O)–H⋯Br hydrogen bonds, generating a supramolecular 3D structure (Fig. S6†).

Compound **2** crystallizes in the noncentrosymmetric monoclinic space group *Cc* (no. 9). The asymmetric unit consists of one antimony atom, five bromine atoms, and two protonated nicotinic molecules. The antimony atom is surrounded by six bromine atoms with the Sb–Br bond distance in the range of 2.6167(18)–3.1187(19) Å. The distorted $SbBr_6$ octahedra are interconnected by common vertices to give rise to zigzag chains running along the [001] direction. The two independent protonated nicotinic molecules form a dimeric aggregate though O–H⋯O=C hydrogen bonds with a typical eight-membered-ring motif. They connect the antimony bromide chains through extensive N–H⋯Br hydrogen bonds, forming a supramolecular 3D structure (Fig. S7†).

The noncentrosymmetric structure of compound **2** prompts us to evaluate its NLO properties by the Kurtz–Perry method.[14] The SHG tests were carried out on its sieved powder samples under 1064 nm laser irradiation. The notable NLO material KDP with the same particle size was used as a reference. The SHG response of compound **2** increases with increasing the particle size in the range of 25 to 212 μm, indicating that the compound is type I phase-matchable (Fig. 2a). In particular, the SHG efficiency of compound **2** is found to be 3.7 times that of KDP with the particle size distributions ranging from 150 to 212 μm (Fig. 2b). Such a strong SHG effect is remarkable among organic–inorganic hybrid antimony halide perovskites (Fig. 2c). For example, the SHG efficiencies are 0.67× KDP for [*N*,*N*-dimethyl-1,3-propanediamine]$SbBr_5$, 1.7× KDP for $(C_9N_3H_{15})(C_9H_{13}SO)SbBr_6$, 2.1× KDP for $(C_9H_{14}N)SbCl_4$, and 2.6× KDP for L-H_2his·$SbBr_5$·H_2O, respectively, under 1064 nm laser irradiation.[5,15]

The SHG effect of compound **2** is closely related to its structural distortion. Generally, the large distortions of MX_6 octahedra in metal halide perovskites will lead to large polarization, which is beneficial for a strong SHG response. Herein, the distorted level (Δd) of the $SbBr_6$ octahedron of compound **2** is calculated by the following eqn (1):

$$\Delta d = \frac{1}{6}\sum_{n=1}^{6}[(d_n - d)/d]^2 \qquad (1)$$

where d_n represents the six individual Sb–Br bond lengths (Table S1†) and d represents the mean Sb–Br bond length. The

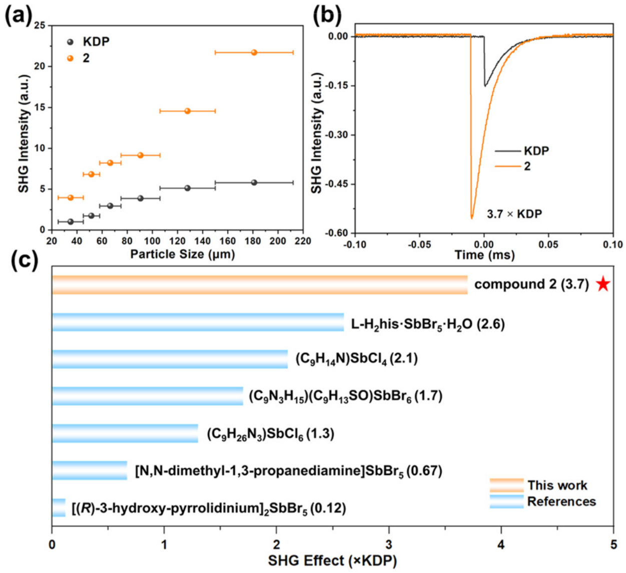

Fig. 2 (a) SHG intensity *versus* particle size for compound **2** and KDP. (b) Oscilloscope traces of the SHG signals of compound **2** and KDP. (c) Comparison of the SHG effects of several organic–inorganic hybrid antimony halide perovskites under 1064 nm laser irradiation.

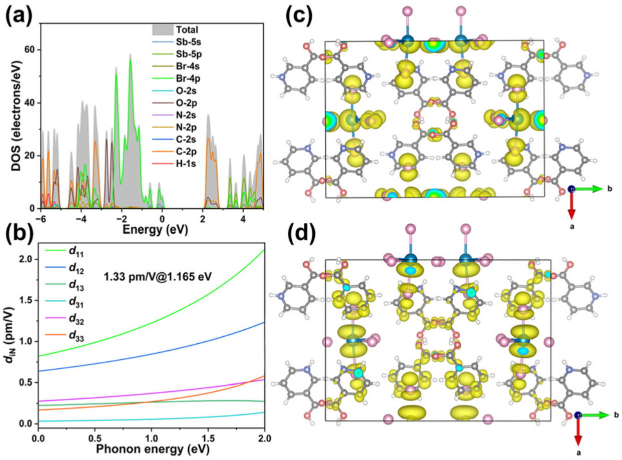

Fig. 3 (a) Total and partial DOS for compound **2**. (b) Calculated frequency-dependent SHG coefficients for compound **2**. SHG-weighted densities of compound **2** for (c) occupied and (d) unoccupied states in the virtual electron process.

value of Δ*d* is calculated to be 5.96 × 10^{-3} for compound **2**, which is slightly larger than those of antimony halide perovskites, such as [*N*,*N*-dimethyl-1,3-propanediamine]SbBr$_5$ (1.400 × 10^{-3}) and (C$_9$N$_3$H$_{15}$)(C$_9$H$_{13}$SO)SbBr$_6$ (1.576 × 10^{-3}).[15a,b]

To gain a better understanding of the optical properties of compounds **1** and **2**, the theoretical calculations were carried out by the density functional theory (DFT).[16] The electronic band structures of the two compounds are shown in Fig. S8.† The highest valence bands (VB) for compound **1** is located at the point Q and the lowest conduction bands (CB) is located at the point G, indicating that compound **1** has an indirect band gap. For compound **2**, both the highest VB and the lowest CB are located at the point G, indicating that it is a direct-gap material. Their optical band gaps are calculated to be 2.28 and 2.19 eV, respectively, which are a bit less than the experimental values. The total and partial densities of states (DOS) analysis shows that the top of VB is mainly attributed to the contributions from the Sb 5s and Br 4p orbitals, while the bottom of CB is mostly from the C 2p, N 2p, and O 2p orbitals (Fig. 3a and Fig. S9†). Hence, the band gaps of compounds **1** and **2** are determined by the distorted SbBr$_n$ (n = 5, 6) polyhedra and nicotinic acids. The refractive index dispersion curves display an appropriate anisotropy and follow the order of $n_z > n_y > n_x$, indicating that compounds **1** and **2** are biaxial crystals (Fig. S10†). The calculated birefringence values are 0.099 at 546 nm for compound **1** and 0.048 at 546 nm for compound **2**, which are consistent with the experimental results.

Under the restriction of Kleinman symmetry, compound **2** has six non-zero independent SHG coefficients, d_{11}, d_{12}, d_{13}, d_{31}, d_{32}, and d_{33}, with calculated values of 1.33, 0.89, 0.27, 0.06, 0.39, and 0.30 pm V^{-1}, respectively. Notably, the largest value for d_{11} is approximately 3.4 times that of KDP (d_{36} = 0.39 pm V^{-1}), which matches well with the experimental result (Fig. 3b). To elucidate the source of the SHG effect, the SHG-weighted electron densities of the largest tensor d_{11} were performed.[17] The occupied and unoccupied states of the virtual electron process for compound **2** are presented in Fig. 3c and d. For the occupied states, the SHG-weighted electron clouds are localized on the Sb and Br atoms of the SbBr$_6$ octahedra. For the unoccupied states, the distorted SbBr$_6$ octahedra dominate the SHG contribution and the nicotinic acid molecules make the minor contribution. A real-space atomic cutting analysis shows that the contribution from the SbBr$_6$ octahedra to the SHG effect of compound **2** is 73.0%, while the contribution from the nicotinic acid molecules to the SHG effect is 27.0%.[18] Therefore, the SHG effect in compound **2** should originate from the synergistic effect of the distorted SbBr$_6$ octahedra and planar nicotinic acid molecules.

In summary, two new organic–inorganic hybrid antimony bromides have been synthesized by a solvent evaporation method. Although both compounds contain the same organic cations as structure-directing agents, they feature different structural dimensionalities: 0D tetranuclear cluster for compound **1** and 1D zigzag chain for compound **2**. Notably, compound **2** exhibits a strong SHG response of 3.7× KDP originating from the synergistic effect of the distorted SbBr$_6$ octahedra and planar nicotinic acid molecules. This work demonstrates the great potential of pyridinecarboxylic acids in synthesizing organic–inorganic hybrid metal halide perovskites with strong SHG effects.

Conflicts of interest

There are no conflicts to declare.

Data availability

The data supporting this article have been included as part of the ESI.† Crystallographic data for compounds **1** and **2** have been deposited at the CCDC under 2456325 and 2456326.†

Acknowledgements

This work was supported by the Institutional Research Fund from Sichuan University (no. 2023SCUH0077). We thank Dr Daichuan Ma from the Analytical & Testing Center at Sichuan University for his contributions to the theoretical calculations.

References

‡ Crystal data for **1**: $C_{12}H_{14}Br_8N_2O_5Sb_2$: M = 1149.03, triclinic, space group $P\bar{1}$ (no. 2), a = 11.9799(3) Å, b = 12.1232(3) Å, c = 12.1910(4) Å, α = 100.822(1)°, β = 109.348(1)°, γ = 116.842(1)°, V = 1365.66(7) Å^3, Z = 2, D_c = 2.794 g cm^{-3}, μ = 13.706 mm^{-1}, 37 041 reflections measured, 6265 unique (R_{int} = 0.0643). The final wR_2 (all data) = 0.1383, final R_1 = 0.0466. Crystal data for **2**: $C_{12}H_{12}Br_5N_2O_4Sb$: M = 769.54, monoclinic, space group Cc (no. 9), a = 14.0673 (8) Å, b = 19.4421 (8) Å, c = 8.0411(6) Å, β = 98.518(3)°, V = 2175.0(2) Å^3, Z = 4, D_c = 2.350 g cm^{-3}, μ = 10.471 mm^{-1}, 16 823 reflections measured, 4205 unique (R_{int} = 0.0912). The final wR_2 (all data) = 0.1262, final R_1 = 0.0498.

1 (*a*) B. Saparov and D. B. Mitzi, *Chem. Rev.*, 2016, **116**, 4558; (*b*) P. F. Gong, F. Liang, L. Kang, X. G. Chen, J. G. Qin, Y. C. Wu and Z. S. Lin, *Coord. Chem. Rev.*, 2019, **380**, 83; (*c*) K. Ding, H. S. Ye, C. Y. Su, Y. A. Xiong, G. W. Du, Y. M. You, Z. X. Zhang, S. Dong, Y. Zhang and D. W. Fu, *Nat. Commun.*, 2023, **14**, 2863; (*d*) Y. S. Zheng, X. Han, P. X. Cheng, X. D. Jia, J. L. Xu and X. H. Bu, *J. Am. Chem. Soc.*, 2022, **144**, 16471; (*e*) C. C. Stoumpos, L. Frazer, D. J. Clark, Y. S. Kim, S. H. Rhim, A. J. Freeman, J. B. Ketterson, J. I. Jang and K. G. Kanatzidis, *J. Am. Chem. Soc.*, 2015, **137**, 6804; (*f*) Y. Liu, Y. P. Gong, S. N. Geng, M. L. Feng, D. Manidaki, Z. Y. Deng, C. C. Stoumpos, P. Canepa, Z. W. Xiao, W. X. Zhang and L. L. Mao, *Angew. Chem., Int. Ed.*, 2022, **61**, e202208875; (*g*) S. Choi, Y. Li, Y. Kuk and K. M. Ok, *Adv. Sci.*, 2025, **12**, 2414503; (*h*) T. T. Tran, H. Yu, J. M. Rondinelli, K. R. Poeppelmeier and P. S. Halasyamani, *Chem. Mater.*, 2016, **28**, 5238.

2 (*a*) Q. R. Shui, H. X. Tang, R. B. Fu, Y. B. Fang, Z. J. Ma and X. T. Wu, *Angew. Chem., Int. Ed.*, 2021, **60**, 2116; (*b*) P. X. Cheng, X. D. Jia, S. Q. Chai, G. Li, M. Y. Xin, J. J. Guan, X. Han, W. Q. Han, S. M. Zeng, Y. S. Zheng, J. L. Xu and X. H. Bu, *Angew. Chem., Int. Ed.*, 2024, **63**, e202400644; (*c*) L. L. Zhang, Q. R. Ding, P. H. Wang, Y. Q. Zhang, Q. Y. Liu, Y. L. Wang and J. H. Luo, *Inorg. Chem. Front.*, 2024, **11**, 3618; (*d*) C. K. Yang, W. N. Chen, Y. T. Ding, J. Wang, Y. Rao, W. Q. Liao, Y. Y. Tang, P. F. Li, Z. X. Wang and R. G. Xiong, *Adv. Mater.*, 2019, **31**, 1808088; (*e*) J. Cheng, G. J. Yi, P. Q. Qian, J. Li, L. Huang, H. M. Zeng, G. H. Zou and Z. E. Lin, *Inorg. Chem.*, 2024, **63**, 15579; (*f*) J. Z. Li, Z. H. Guo, M. T. Wang, Y. H. Shao, Y. Chen, Y. Qin, W. J. Zhang, C. S. Wang, H. Jin, L. Y. Wang and T. C. He, *Laser Photonics Rev.*, 2025, **19**, 2401379.

3 (*a*) D. Y. Fu, J. L. Xin, Y. Y. He, S. C. Wu, X. Y. Zhang, X. M. Zhang and J. H. Luo, *Angew. Chem., Int. Ed.*, 2021, **60**, 20021; (*b*) Y. S. Zheng, J. L. Xu and X. H. Bu, *Adv. Opt. Mater.*, 2022, **10**, 2101545; (*c*) J. Cheng, G. J. Yi, Z. Z. Zhang, Y. Long, H. M. Zeng, L. Huang, G. H. Zou and Z. E. Lin, *Angew. Chem., Int. Ed.*, 2024, **63**, e202318385.

4 (*a*) X. L. Zhao, N. Wang, M. Z. Quan, A. Hou, K. J. Liu, Y. B. Cui, J. Zhao and Q. L. Liu, *Inorg. Chem.*, 2024, **63**, 10705; (*b*) D. Chen, F. L. Dai, S. Q. Hao, G. J. Zhou, Q. L. Liu, C. Wolverton, J. Zhao and Z. G. Xia, *J. Mater. Chem. C*, 2020, **8**, 7322.

5 X. M. Wen, J. Cheng, P. Q. Qian, Z. Z. Zhang, H. M. Zeng, L. Huang, G. H. Zou and Z. E. Lin, *Dalton Trans.*, 2024, **53**, 260.

6 (*a*) Z. Y. Ba, J. Lee, H. Kim, C. L. Hu and K. M. Ok, *Small*, 2023, **19**, 2301756; (*b*) L. H. Liu, Z. Y. Bai, L. Hu, D. S. Wei, Z. B. Lin and L. Z. Zhang, *J. Mater. Chem. C*, 2021, **9**, 7452; (*c*) Y. W. Kang, C. Yang, J. Gou, Y. L. Zhu, Q. W. Zhu and Q. Wu, *Inorg. Chem.*, 2024, **63**, 2725; (*d*) Y. B. Cui, J. D. Cao, J. W. Lin, C. X. Li, J. Y. Yao, K. J. Liu, A. Hou, Z. N. Guo, J. Zhao and Q. L. Liu, *Dalton Trans.*, 2024, **53**, 10235; (*e*) J. J. Wu, Y. F. Fu, W. L. Liu and S. P. Guo, *Inorg. Chem. Front.*, 2024, **11**, 7090; (*f*) J. Cheng, G. J. Yi, Y. Long, Q. L. Zhong, G. H. Zou, L. D. Luan and Z. E. Lin, *Dalton Trans.*, 2025, **54**, 10351.

7 (*a*) M. Mutailipu, J. Han, Z. Li, F. M. Li, J. J. Li, F. F. Zhang, X. F. Long, Z. H. Yang and S. L. Pan, *Nat. Photonics*, 2023, **17**, 694; (*b*) D. M. Wang, Z. Z. Wei, Z. Y. Bai, L. H. Liu, Z. B. Lin and L. Z. Zhang, *Dalton Trans.*, 2022, **51**, 463; (*c*) M. Luo, C. S. Lin, D. H. Lin and N. Ye, *Angew. Chem., Int. Ed.*, 2020, **59**, 15978; (*d*) C. Wu, X. X. Jiang, Z. J. Wang, H. Y. Sha, Z. S. Lin, Z. P. Huang, X. F. Long, M. G. Humphrey and C. Zhang, *Angew. Chem., Int. Ed.*, 2021, **60**, 14806.

8 (*a*) J. Gou, Y. L. Zhu, X. Su, C. Yang, Y. J. Wang, Q. W. Zhu, Y. Xiong and Q. Wu, *Inorg. Chem. Front.*, 2025, **12**, 3595; (*b*) J. H. Wu, C. L. Hu, Y. F. Li, J. G. Mao and F. Kong, *Chem. Sci.*, 2024, **15**, 8071; (*c*) L. Qi, X. X. Jiang, K. Duanmu, C. Wu, Z. S. Lin, Z. P. Huang, M. G. Humphrey and C. Zhang, *J. Am. Chem. Soc.*, 2024, **146**, 9975; (*d*) S. M. Qi, P. X. Cheng, X. Han, F. Ge, R. C. Shi, L. Xu, G. Li and J. L. Xu, *Cryst. Growth Des.*, 2022, **22**, 6545; (*e*) J. Lu, X. Liu, M. Zhao, X. B. Deng, K. X. Shi, Q. R. Wu, L. Chen and L. M. Wu, *J. Am. Chem. Soc.*, 2021, **143**, 3647.

9 C. Y. Shen, J. Liu, D. F. Sun, K. Yang, B. B. Zhang, K. Wu, J. Y. Wang and D. L. Wang, *Small*, 2025, **21**, 2501471.

10 X. Y. Li, Q. Wei, C. L. Hu, J. Pan, B. X. Li, Z. Z. Xue, X. Y. Li, J. H. Li, J. G. Mao and G. M. Wang, *Adv. Funct. Mater.*, 2023, **33**, 2210718.

11 C. Wang, T. Zhang and W. B. Lin, *Chem. Rev.*, 2012, **112**, 1084.

12 (*a*) D. P. Chen, Z. X. Song, C. Yang, Y. Y. Wei, G. K. Liu, L. Q. Meng, Q. Wu and Y. Y. Dang, *Inorg. Chem.*, 2024, **63**, 10304; (*b*) Z. K. Qi, Y. L. Chen, H. Z. Gao, F. Q. Zhang,

S. L. Li and X. M. Zhang, *Sci. China: Chem.*, 2021, **64**, 2111; (*c*) W. J. Wei, H. Q. Gao, Y. Yang, M. Fang, X. D. Wang, X. Chen, W. L. Qin, G. Q. Chen, R. X. Li, Y. Z. Tang and Y. Wei, *Chem. Mater.*, 2022, **34**, 6323.

13 (*a*) F. Ge, P. X. Cheng, Q. W. Li, J. L. Xu and X. H. Bu, *Adv. Opt. Mater.*, 2023, **11**, 2301040; (*b*) A. Piecha, A. Białońska, R. Jakubas and W. Medycki, *Solid State Sci.*, 2008, **10**, 1469.

14 S. K. Kurtz and T. T. Perry, *J. Appl. Phys.*, 1968, **39**, 3798.

15 (*a*) Z. Q. Peng, P. Wang, Z. H. Wei, W. J. Guo, H. N. Zhang and H. Cai, *Inorg. Chem.*, 2024, **63**, 184; (*b*) J. D. Cao, K. J. Liu, M. Z. Quan, A. Hou, X. X. Jiang, Z. S. Lin, J. Zhao and Q. L. Liu, *Dalton Trans.*, 2023, **52**, 9368; (*c*) F. F. Wu, Q. Y. Wei, X. Q. Li, Y. Liu, W. Q. Huang, Q. Chen, B. X. Li, J. H. Luo and X. T. Liu, *Cryst. Growth Des.*, 2022, **22**, 3875; (*d*) J. Cheng, P. Q. Qian, M. Yang, L. Huang, H. M. Zeng, G. H. Zou and Z. E. Lin, *Inorg. Chem.*, 2023, **62**, 16673; (*e*) H. Y. Shen, L. He, P. P. Shi and Q. Ye, *J. Mater. Chem. C*, 2021, **9**, 4338.

16 (*a*) A. Tkatchenko and M. Scheffler, *Phys. Rev. Lett.*, 2009, **102**, 073005; (*b*) H. Mizoguchi and P. M. Woodward, *Chem. Mater.*, 2004, **16**, 5233.

17 (*a*) H. X. Fan, C. S. Lin, F. Liang, H. T. Tian, S. J. Huang, Y. Q. Zhou, S. X. Ke, B. X. Li, N. Ye and M. Luo, *ACS Appl. Mater. Interfaces*, 2022, **14**, 32270; (*b*) R. He, Z. S. Lin, M. H. Lee and C. T. Chen, *J. Appl. Phys.*, 2011, **109**, 103510.

18 (*a*) Z. S. Lin, X. X. Jiang, L. Kang, P. F. Gong, S. Y. Luo and M. H. Lee, *J. Phys. D: Appl. Phys.*, 2014, **47**, 253001; (*b*) J. Lin, M. H. Lee, Z. P. Liu, C. T. Chen and C. J. Pickard, *Phys. Rev. B*, 1999, **60**, 13380.